Problems in the Classic Frequency Shift Islanding Detection Methods Applied to Energy Storage Converters and a Coping Strategy

Menghua Liu, Wei Zhao, Songling Huang, Qing Wang, *Senior Member, IEEE,* and Kunpeng Shi

***Abstract*—This paper first derives a usable formula based on the parallel *R*, *L*, *C* load and the conclusions from frequency shift islanding detection methods in current literature: the angle by which the total output current of the distributed resources (DR) units leads the point of common coupling (PCC) voltage must be conducted to have the same shifting direction as the load admittance angle during the variation of the frequency. On the basis of the formula and multi-DR operation, the scenarios in which the classic frequency shift methods are applied to energy storage converters are analyzed. The results indicate that the setting of the angle by which the energy storage converter current leads the PCC voltage may need to be modified when running state changes. It results in the problems that the classic methods are not applicable for non-UPF (unity power factor) control and have to distinguish between generation mode and consumption mode for UPF control. On account of the problems, a coping strategy, i.e. an improved method, is proposed. The analyses indicate that the improved method is applicable in every state. The last simulations and experiments confirm the preceding conclusions.**

***Index terms*—consumption mode, energy storage converter, frequency shift, islanding detection, microgrid, multi-DR, reactive current perturbation**

NOMENCLATURE

DR	distributed resources
PCC	point of common coupling
R, L, C	effective load resistance, inductance and capacitance in an island
SFS	Sandia Frequency Shift
SMS	Slip-Mode Frequency Shift
UPF	unity power factor
f	PCC frequency
f_g	nominal frequency of a power grid
$\dot{I}_c$	total currents vector of the DR units
$\dot{I}_{con}$	output current vector of the energy storage converter
i_{dref}	active current reference value
I_{iA}	amplitude of the rated current of the energy storage converter
$\dot{I}_{inv}$	output current vector of the inverter
i_{invq}	projection of $\dot{I}_{inv}$ on the q-axis
I_p	gain of the perturbation
i_{per}	reactive current perturbation
i_{qref}	reactive current reference value
P	load active power (per-unit)
P_{con}	energy storage converter output active power
P_{qL}	load inductive reactive power (per-unit)
P_{inv}	inverter output active power
Q_{con}	energy storage converter output reactive power
Q_f	load quality factor
Q_{inv}	inverter output reactive power
$\dot{U}_{PCC}$	voltage vector at PCC

M. Liu, W. Zhao, S. Huang, and K. Shi are with the State Key Laboratory of Power System, Department of Electrical Engineering, Tsinghua University, Beijing, 100084, China (e-mail: liumh13@mails.tsinghua.edu.cn; zhaowei@mail.tsinghua.edu.cn; huangsling@tsinghua.edu.cn; kunpengshi2005@163.com).

Q. Wang is with the School of Engineering and Computing Sciences, Durham University, U.K. (qing.wang@durham.ac.uk).

θ_0 angle expected by control system

θ_c reference angle by which the total output current of DR units leads the PCC voltage

θ_{con} angle by which $\dot{I}_{con}$ leads $\dot{U}_{PCC}$

θ_d perturbing angle in the improved method

θ_f perturbing angle in the classic methods

θ_L load admittance angle

I. Introduction

Islanding detection has attracted much research since it was first introduced. The detection methods aimed at it include remote schemes and local schemes, the latter of which are divided into passive methods and active methods. The active methods have received more attention due to their advantages in expense and performance. Two famous ones are Sandia Frequency Shift (SFS) and Slip-Mode Frequency Shift (SMS), which belong to frequency shift methods and have been the classic active islanding detection methods up to the present day [1]-[6]. In addition, [7] and [8] proposed two methods based on the relationships between reactive power and frequency; [9] and [10] added a reactive power perturbation on the basis of SMS and SFS; [11] proposed a method based on a relationship between active power and voltage; [12] proposed the concept of perturbing reactive current, and [13]-[15] realized and tested it. Although new methods are constantly emerging, SFS and SMS are still being widely used. Hence, this paper focuses on these two classic methods.

The classic methods can function well in single-DR (distributed resources) operation. However, obviously, they are more commonly utilized in multi-DR operation where some problems may emerge. [16] shows the interactions between different frequency shift methods in multi-DR operation. [17] and [18] reveal the interactions between SFS methods and propose a technique to reduce the non-detection zone. However, the scenarios in consumption mode are rarely discussed [19][20].

On the basis of multi-DR operation, this paper analyzes different running states, including that in consumption mode. Through the analyses it can be found that the classic methods have significant problems on parameter setting, even without considering the interactions between them, which results in such methods not applicable for non-UPF (unity power factor) control and having to distinguish between generation mode and consumption mode for UPF control. This paper will center on the problems.

This paper is organized as follows. In section II, a usable formula for frequency shift methods is proposed. Section III analyses several scenarios and finds the problems of the classic methods according to the formula. In view of the problems, a coping strategy, i.e. an improved method, is proposed in section IV. Section V and section VI verify the previous analyses by simulations and experiments, respectively. Section VII draws a conclusion for this paper.

II. A Usable Formula For Frequency Shift Methods

Parallel *R*, *L*, *C* load is the test model in IEEE Std 1547.1-2005 [21]. Hence, it is the default load in this paper. Fig. 1 shows a diagram of the Multi-DR operation. In some areas, especially where a microgrid has been constructed, both generation facilities (e.g. inverters) and storage facilities (e.g. energy storage converters) are equipped [22][23], and this is the situation that will be discussed in this paper.

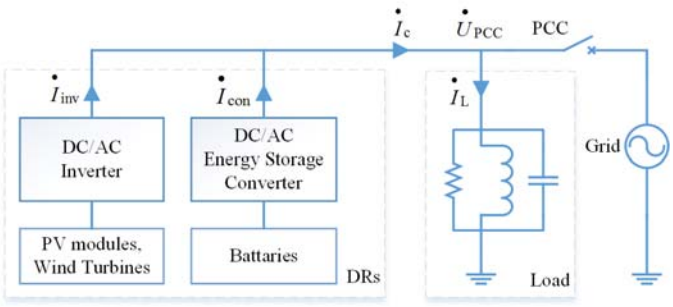

Fig. 1. Multi-DR operation

References [24] and [25] have indicated that if (1) is satisfied in an island condition, the frequency at the point of common coupling (PCC) will continuously change.

$$\mathrm{d}\theta_c/\mathrm{d}f > \mathrm{d}\theta_L/\mathrm{d}f \tag{1}$$

where θ_c represents the reference angle by which the total output current of DR units (i.e. $\dot{I}_c$) leads the PCC voltage (i.e. $\dot{U}_{PCC}$), so that it is different from the actual angle in an island condition, and θ_L represents the load admittance angle.

References [26] and [24] have pointed out that if the DR units reaches a new steady state in an island condition, (2), which is called the phase criterion, will be satisfied.

$$\theta_c=\theta_L \tag{2}$$

By uniting (1) and (2), (3) can be established on a steady state of an island, i.e. a necessary condition for the frequency stabilization.

$$\left.\begin{array}{l}\theta_c = \theta_L \\ \mathrm{d}\theta_c/\mathrm{d}f < \mathrm{d}\theta_L/\mathrm{d}f\end{array}\right\} \tag{3}$$

Frequency shift methods are there to make *f* deviate from the limits in an island condition. In (3), θ_c can be controlled by DRs, thus, so long as θ_c does not satisfy (3), *f* will continuously change up to deviating from the limits. Specifically, at least one of (1) and (4) must be ensured for a frequency shift method.

$$\theta_c\neq\theta_L \tag{4}$$

With regard to parallel *R*, *L*, *C* load, θ_L is

$$\theta_{\mathrm{L}} = \arctan[R(2\pi fC - \frac{1}{2\pi fL})] .$$

The derivative of θ_{L} is

$$\frac{\mathrm{d}\theta_{\mathrm{L}}}{\mathrm{d}f} = \frac{2\pi RC + \frac{R}{2\pi Lf^2}}{1 + R^2(2\pi fC - \frac{1}{2\pi fL})^2}$$

There is $\mathrm{d}\theta_{\mathrm{L}}/\mathrm{d}f \geq 0$. For satisfying (1), (5) is necessary.

$$\mathrm{d}\theta_{\mathrm{c}}/\mathrm{d}f > 0 \tag{5}$$

For parallel R, L, C load, θ_{L} may spontaneously move towards θ_{c} when an island is present, otherwise f cannot tend to stabilization since (2) cannot be satisfied. Then if θ_{c} is shifted in the same direction as θ_{L} during f variation to meet (4), f will continuously change. This is an intuitive statement of why (5) is necessary. Although (5) cannot completely ensure (1), it points out the sign of $\mathrm{d}\theta_{\mathrm{c}}/\mathrm{d}f$, which is important for the analyses below. As regards the size of $\mathrm{d}\theta_{\mathrm{c}}/\mathrm{d}f$, [24] and [25] have presented the design criteria which aim at completely satisfying (1). Then, a usable formula can be derived: θ_{c} must have the same shifting direction as θ_{L} during the frequency variation. Due to $\mathrm{d}\theta_{\mathrm{L}}/\mathrm{d}f \geq 0$, (5) just reflects the formula.

III. The Classic Frequency Shift Methods Applied To Energy Storage Converters On The Basis Of The Usable Formula

This section will introduce the mentioned formula into the classic methods which are employed by the energy storage converter [1]. In power matching or near matching conditions islanding detection is difficult, thus it is more meaningful to analyze an islanding detection method in such conditions. The total active power of the DR units is appointed to be positive, so that the load power may be matched. The inverter operates in generation mode, whereas the energy storage converter can operate in generation mode or consumption mode. In fact, even if the inverter operates in consumption mode, the last conclusions can still be obtained as long as the total output active power of the DR units is positive. To simplify the analyses and stress a focal point, this paper assumes that only the energy storage converter takes charge of islanding detection, which will not affect the final conclusion.

A. UPF Control

1) Generation mode

Fig. 2. shows a vector diagram of currents and voltage of the DR units in the d-q synchronous reference frame in an island condition.

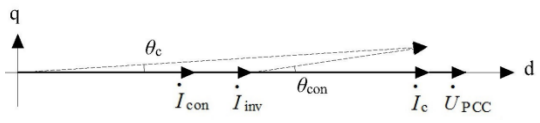

Fig. 2. Vector diagram in generation mode and UPF control

In Fig. 2, $\dot{U}_{\mathrm{PCC}}$ is the voltage vector at PCC; $\dot{I}_{\mathrm{con}}$ and $\dot{I}_{\mathrm{inv}}$ represent the output current vectors of the energy storage converter and the inverter, respectively; $\dot{I}_{\mathrm{c}}$ represents the total currents vector of the DR units. Then there is the following relationship (see Fig. 1).

$$\dot{I}_{\mathrm{c}} = \dot{I}_{\mathrm{con}} + \dot{I}_{\mathrm{inv}}$$

According to (5), there is

$$\mathrm{d}\theta_{\mathrm{c}}/\mathrm{d}\theta_{\mathrm{con}} \cdot \mathrm{d}\theta_{\mathrm{con}}/\mathrm{d}f > 0 \tag{6}$$

where θ_{con} represents the angle by which $\dot{I}_{\mathrm{con}}$ leads $\dot{U}_{\mathrm{PCC}}$ and can be controlled by the energy storage converter.

As shown in Fig. 2, if θ_{con} is slightly perturbed by implementing the classic methods, there is

$$\mathrm{d}\theta_{\mathrm{c}}/\mathrm{d}\theta_{\mathrm{con}} > 0$$

According to (6), the following relationship is required.

$$\mathrm{d}\theta_{\mathrm{con}}/\mathrm{d}f > 0 \tag{7}$$

In other words, for the classic methods, in order to comply with the mentioned formula θ_{con} must be set as (7).

2) Consumption mode

As shown in Fig. 3, in the same way, if θ_{con} is slightly perturbed, there is

$$\mathrm{d}\theta_{\mathrm{c}}/\mathrm{d}\theta_{\mathrm{con}} < 0$$

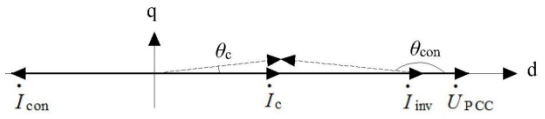

Fig. 3. Vector diagram in consumption mode and UPF control

According to (6), the following relationship is required.

$$\mathrm{d}\theta_{\mathrm{con}}/\mathrm{d}f < 0 \tag{8}$$

Thus, θ_{con} must be set as (8).

B. Non-UPF Control

With the increase of the penetration of distributed generation, some further capabilities are required, such as providing an ancillary service, which needs dispatching reactive power. Accordingly, the DR units may be utilized to satisfy the reactive power requirement [27]-[32]. The following part will analyze the DR units operating in non-UPF control.

1) Generation mode

Fig. 4 shows two vector diagrams in an island condition. The classic methods, in fact, carry out an inverse Givens transformation of the reference currents, shown as (9) [1]. If f

varies, the phase of $\dot{I}_{con}$ will change while the amplitude will not, so that the end point of $\dot{I}_c$ will slip on the arc shown in Fig. 4 when f varies.

$$\begin{pmatrix} i_d^* \\ i_q^* \end{pmatrix} = \begin{pmatrix} \cos\theta_f & -\sin\theta_f \\ \sin\theta_f & \cos\theta_f \end{pmatrix} \begin{pmatrix} i_{dref} \\ i_{qref} \end{pmatrix} \tag{9}$$

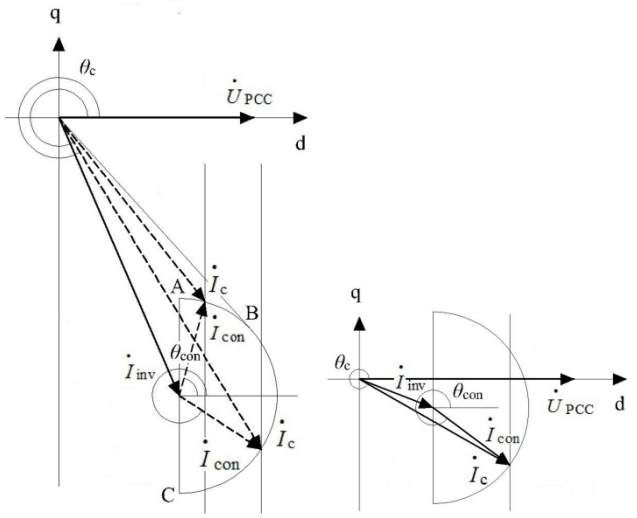

(a) (b)

Fig. 4. Vector diagrams in generation mode and non-UPF control. (a) $|i_{invq}|>I_{con}$. (b) $|i_{invq}|\leq I_{con}$

Fig. 4(a) shows the scenario that $|i_{invq}|>I_{con}$, where i_{invq} is the projection of $\dot{I}_{inv}$ on the q-axis. Point B is the tangent point on the circle relative to the origin (the same as below).

When the end point of $\dot{I}_c$ is on $\overset{\frown}{AB}$, there is

$$d\theta_c/d\theta_{con} < 0$$

According to (6), it can be derived that θ_{con} must be set as (8).

When the end point of $\dot{I}_c$ is on $\overset{\frown}{BC}$, as above, θ_{con} must be set as (7).

The scenario shown in Fig. 4(b) can be analyzed in the same way. The conclusions are summarized in Table I.

TABLE I

SETTING OF θ_{con} IN SCENARIOS SHOWN IN Fig. 4 AND Fig. 5

θ_{con}	Fig. 4(a)	Fig. 4(b)	Fig. 5(a)	Fig. 5(b)	Fig. 5(c)
Set as (7)	$\overset{\frown}{BC}$	Entire arc	$\overset{\frown}{BC}$	$\overset{\frown}{AB_1}$, $\overset{\frown}{B_2C}$	Entire arc (on the right of the q-axis)
Set as (8)	$\overset{\frown}{AB}$		$\overset{\frown}{AB}$	$\overset{\frown}{B_1B_2}$	

2) Consumption mode

Fig. 5 shows three vector diagrams in an island condition. As above, the conclusions are also summarized in Table I.

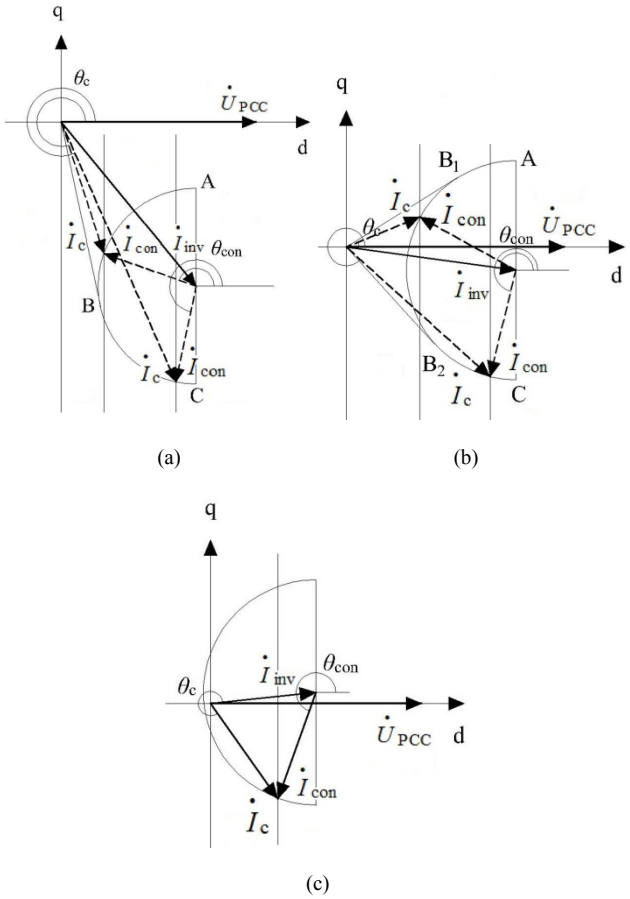

(a) (b)

(c)

Fig. 5. Vector diagram in consumption mode and non-UPF control. (a) $|i_{invq}|>I_{con}$. (b) $|i_{invq}|\leq I_{con}\leq I_{inv}$. (c) $I_{inv}<I_{con}$

For the classic methods, it can be seen from the above analyses that in non-UPF control the setting requirements of θ_{con} are not consistent, which requires the energy storage converter to get the location of the end point of $\dot{I}_c$. Unfortunately, due to the randomness of the occurrence time and region of the island, it is impossible to satisfy the requirement for any local system. That is the problem. Consequently, the classic methods are practicable only in UPF control, and even then, the energy storage converter has to distinguish between generation mode and consumption mode. The next subsection will contribute a modified scheme for consumption mode.

C. A Modified Schemes for $d\theta_{con}/df < 0$

According to the previous conclusions, once the classic frequency shift methods are employed in consumption mode and UPF control, θ_{con} must be set as $d\theta_{con}/df < 0$. The modified schemes to satisfy $d\theta_{con}/df < 0$ are demonstrated below.

For the classic methods, θ_{con} can also be represented as [1][33]

$$\theta_{con}=\theta_0+\theta_f$$

where θ_0 represents the angle expected by the control system

and is independent of f, whereas the perturbing angle θ_f is a function of f. Then the relationship below can be derived.

$$d\theta_{con}/df = d\theta_f/df$$

Therefore, $d\theta_f/df > 0$ must be maintained in generation mode, and in consumption mode $d\theta_{con}/df < 0$ can be realized by modifying θ_f as the negative value of its equivalent in generation mode, i.e. $-\theta_f$.

IV. Coping Strategy—An Improved Method

A. The Principles and Applications of the Improved Method

Compared with the classic methods, the improved method replaces phase angle perturbation with reactive current perturbation. Its implementation scheme is shown in Fig. 6.

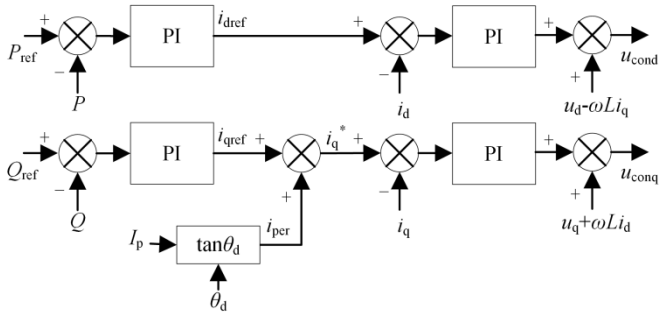

(a)

(b)

Fig. 6. Block diagrams of the improved method. (a) Constant power control. (b) Constant current control

The reactive current perturbation in Fig. 6 is

$$i_{per}=I_p\tan\theta_d \tag{10}$$

where θ_d represents the perturbing angle and is related to f. To decouple the active and reactive current control and enhance the effectiveness of the perturbation, I_p can be set as below:

Constant power control,

$$I_p=I_{iA}$$

Constant current control,

$$I_p=\begin{cases}0.1I_{iA} & 0\le|i_{dref}|<0.1I_{iA}\\ 0.2I_{iA} & 0.1I_{iA}\le|i_{dref}|<0.2I_{iA}\\ \vdots & \vdots\\ I_{iA} & 0.9I_{iA}\le|i_{dref}|\end{cases}$$

where I_{iA} and i_{dref} represent the amplitude of the rated current of the energy storage converter and the active current reference value, respectively.

In contrast with the classic methods, the improved method does not perturb the active current, and there is little coupling between the active and reactive current control. In addition, the improved method transforms the phase angle perturbation (i.e. θ_d) into its equivalent reactive current perturbation (i.e. i_{per}), by which the parameter of the classic methods can be referred, e.g. setting $\theta_d=\theta_f$. At this point it is simpler than some similar methods [13]-[15]. Next, the scenarios for which this method is applied to the energy storage converter will be analyzed.

If the improved method is employed in UPF control, the conclusions are the same as that in section III-A. In non-UPF control, as shown in Fig. 4 and Fig. 5, if f varies, the phase of $\dot{I}_{con}$ will change while the projection of $\dot{I}_{con}$ on the d-axis (i.e. active current) will not, so that the end point of $\dot{I}_c$ will slip on the lines parallel to the q-axis when f varies.

As shown in Fig. 4, in generation mode the relationship below is always established.

$$d\theta_c/d\theta_{con} > 0$$

According to (6), θ_{con} must be set as (7).

As shown in Fig. 5, in consumption mode, as above, θ_{con} must be set as (8).

The specific conclusions on the setting of θ_{con} are summed up in Table II.

TABLE II

Setting of θ_{con}

Conditions	UPF control	Non-UPF control
Generation mode, the classic methods	$d\theta_{con}/df>0$	$d\theta_{con}/df>0$ or $d\theta_{con}/df<0$ (Depend on $\dot{I}_c$)
Consumption mode, the classic methods	$d\theta_{con}/df<0$	$d\theta_{con}/df>0$ or $d\theta_{con}/df<0$ (Depend on $\dot{I}_c$)
Generation mode, the improved method	$d\theta_{con}/df>0$	$d\theta_{con}/df>0$
Consumption mode, the improved method	$d\theta_{con}/df<0$	$d\theta_{con}/df<0$

B. The Specific Scheme Aiming at the Setting of $d\theta_{con}/df$

For the improved method there is

$$d\theta_{con}/df = d\theta_{con}/d(i_{qref}+i_{per}) \cdot d(i_{qref}+i_{per})/df \quad (11)$$

where i_{qref} and $i_{qref}+i_{per}$ represent the reactive current reference value and the projection of $\dot{I}_{con}$ on the q-axis (i.e. reactive current), respectively. Since i_{qref} is independent of f, (11) can also be written as

$$d\theta_{con}/df = d\theta_{con}/d(i_{qref}+i_{per}) \cdot di_{per}/df. \quad (12)$$

As shown in Fig. 2 and Fig. 4, in generation mode there is

$$d\theta_{con}/d(i_{qref}+i_{per}) > 0.$$

According to (12), it can be derived that

$$d\theta_{con}/df > 0 \Leftrightarrow di_{per}/df > 0 .$$

In the same way, as shown in Fig. 3 and Fig. 5, in consumption mode there is

$$d\theta_{con}/df < 0 \Leftrightarrow di_{per}/df > 0 .$$

Thus, (13) must be satisfied whether in generation mode or in consumption mode.

$$di_{per}/df > 0 \quad (13)$$

According to (10), (13) is equivalent to (14).

$$d\theta_{d}/df > 0 \quad (14)$$

Therefore, the setting of θ_{con} can be achieved as long as (14) is satisfied and there is no need to distinguish the running states. In other words, the improved method proposed in this paper is applicable in every state. Compared with the mentioned classic methods, the improved method has obvious advantages.

V. Simulations

The simulations performed on Matlab/Simulink are based on a 220 V/50 Hz single-phase source. The simulation circuit is shown in Fig. 7, where there is a 9 kVA energy storage converter and an inverter connected to the source. Only the energy storage converter implements the islanding detection method. SFS and the improved method will be employed in the following simulations and experiments.

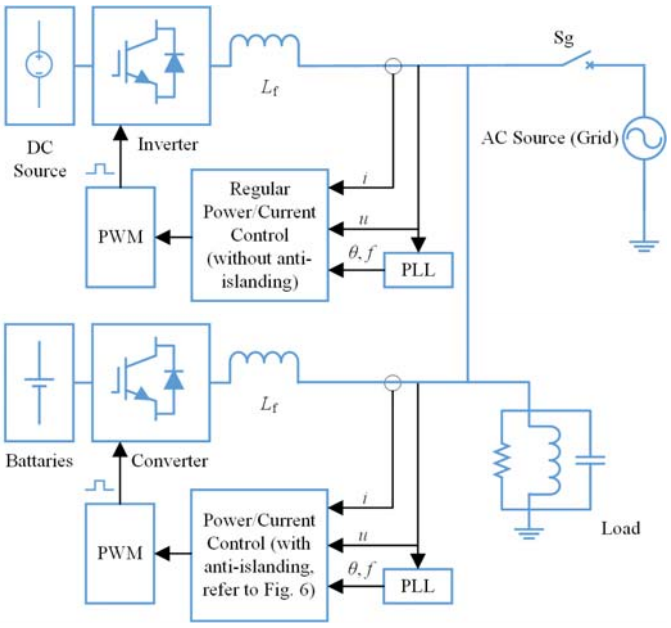

Fig. 7. Simulation circuit

The parameters of SFS and the improved method are listed as below.

$\theta_f = [0.01+0.5(f-f_g)]\pi/2$, for $d\theta_{con}/df > 0$

$\theta_f = -[0.01+0.5(f-f_g)]\pi/2$, for $d\theta_{con}/df < 0$

$\theta_d = [0.01+0.5(f-f_g)]\pi/2$

$I_{iA} = 58$ A

For verifying the effectiveness of the two methods, unless otherwise specified, all the test cases are in power matching conditions. [9] and [1] have demonstrated that in constant power control islanding detection is more difficult, so that the following simulations are based on constant power control. At 0.2 s, switch Sg (see Fig. 7) is disconnected to form an island. The frequency limits depends on the local grid code [34], which is set as 49.5 Hz-50.5 Hz in this paper. The test cases are shown in Table III.

TABLE III

Test Cases in the Simulations

Cases	P_{con} (W)	Q_{con} (Var)	P_{inv} (W)	Q_{inv} (Var)	Corresponding state
UPF, generation mode	2500	0	2500	0	Fig. 2
UPF, consumption mode	-2500	0	7500	0	Fig. 3
Non-UPF, generation mode (The 1st group)	2000	2000	3000	4000	$\overset{\frown}{BC}$ of Fig. 4(a)
Non-UPF, consumption mode (The 1st group)	-5000	1000	10000	5000	$\overset{\frown}{B_1B_2}$ of Fig. 5(b)

Non-UPF, generation mode (The 2nd group)	1000	-3000	4000	9000	$\overset{\frown}{AB}$ of Fig. 4(a)
Non-UPF, consumption mode (The 2nd group)	-1000	5000	6000	1000	$\overset{\frown}{B_2C}$ of Fig. 5(b)

P_{con} and Q_{con} represent the energy storage converter active power and reactive power, respectively, while P_{inv} and Q_{inv} represent the inverter active power and reactive power, respectively.

A. UPF Control

Load parameters: R=9.68 Ω, L=12.3 mH, C=0.822 mF.

The results are shown in Fig. 8, where curves f_1-f_3 and f_4-f_6 are obtained in generation mode and consumption mode, respectively. f_1 and f_4 correspond to the improved method; f_2 and f_5 correspond to the SFS method with $d\theta_{con}/df > 0$, whereas f_3 and f_6 correspond to $d\theta_{con}/df < 0$ (the same below).

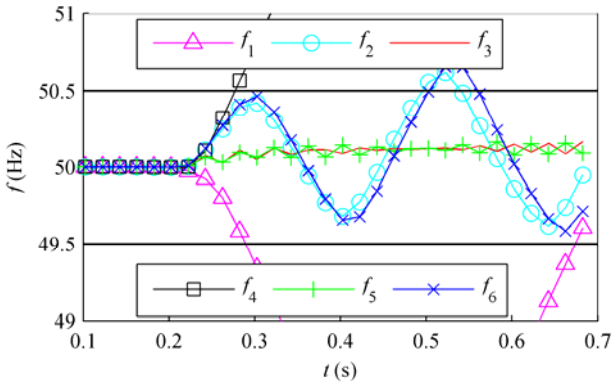

Fig. 8. Frequency waveforms in UPF control. f_1: the improved method in generation mode; f_2: SFS in generation mode with $d\theta_{con}/df > 0$; f_3: SFS in generation mode with $d\theta_{con}/df < 0$; f_4: the improved method in consumption mode; f_5: SFS in consumption mode with $d\theta_{con}/df > 0$; f_6: SFS in consumption mode with $d\theta_{con}/df < 0$ (the same as below)

B. Non-UPF Control

Load parameters: R=9.68 Ω, L=9.72 mH, C=0.648 mF.

The results of the 1st group cases and the 2nd group cases are shown in Fig. 9 and Fig. 10, respectively.

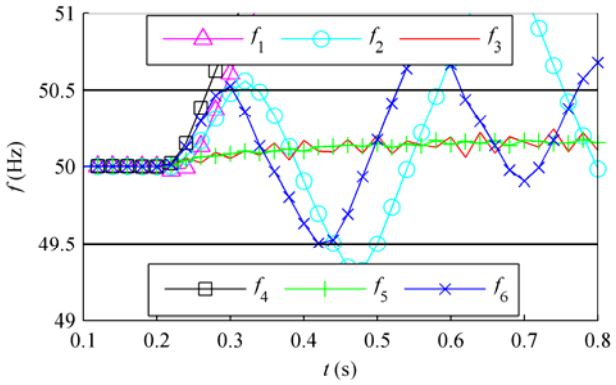

Fig. 9. The 1st group frequency waveforms in non-UPF control

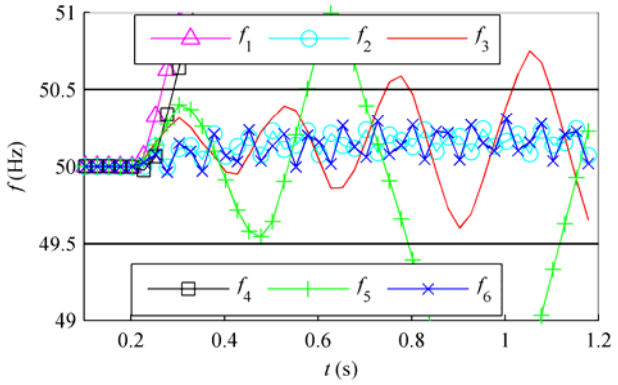

Fig. 10. The 2nd group frequency waveforms in non-UPF control

Fig. 8-Fig. 10 show that the improved method can detect the island in every case, whereas SFS succeeds only when θ_f is set correctly. For SFS, although the cases corresponding to the curves f_2 and f_6 of Fig. 8 are both based on UPF control, to detect the island the settings of θ_f are different due to the different operation mode (generation/consumption mode), and as shown in Fig. 9 and Fig. 10, although the cases corresponding to them are both based on non-UPF control, to detect the island, in the cases of Fig. 9 the setting of θ_f is the same as that in the UPF cases (see Fig. 8), whereas in the cases of Fig. 10 it is just the opposite.

The above simulations confirm the statements in Table II, and demonstrate the universality of the improved method.

C. IEEE Std 1547.1 Testing for the Improved Method

To further evaluate the improved method, this subsection shows six cases with longer trip times, listed in Table IV, which are based on IEEE Std 1547.1. The differences with the above simulations are that only the energy storage converter operates (i.e. single-DR operation) and the island condition is present at 0.35 s.

TABLE IV

TEST CASES BASED ON IEEE STD 1547.1

Cases	P(%)	P_{qL}(%)	R(Ω)	L(mH)	C(mF)	Q_f
1	100	100	5.38	6.85	1.48	2.5
2	100	99	5.38	6.92	1.48	2.49
3	100	101	5.38	6.78	1.48	2.51
4	33	100	16.13	20.54	0.4933	2.5
5	66	100	8.067	10.27	0.9866	2.5
6	66	99	8.067	10.37	0.9866	2.49

P and P_{qL} represent the active load power and inductive reactive power, respectively; while R, L, C and Q_f represent load and quality factor, respectively.

The results shown in Fig. 11 indicate that the frequency can deviate from the limits within 0.45 s, which qualifies for anti-islanding.

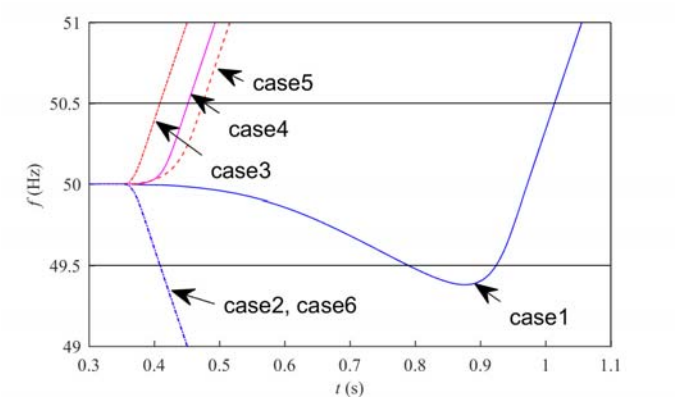

Fig. 11. IEEE Std 1547.1 testing

VI. Experiments

The experimental platform consists of a 5 kVA three-phase energy storage converter and a 5 kVA three-phase inverter, both of which are connected to a 190 V/50 Hz power interface. The configurations of the platform are similar to that of the simulation model above. The parameters of the islanding detection methods are set as below:

$\theta_f = [0.01+0.2(f-f_g)]\pi/2$, for $d\theta_{con}/df > 0$

$\theta_f = -[0.01+0.2(f-f_g)]\pi/2$, for $d\theta_{con}/df < 0$

$\theta_d = [0.01+0.2(f-f_g)]\pi/2$

$I_{iA} = 21$ A

To compare with the above simulations as well as to be not verbose, two cases shown in Table V are tested.

TABLE V

Test Cases in the Experiments

Cases	P_{con} (W)	Q_{con} (Var)	P_{inv} (W)	Q_{inv} (Var)	Corresponding state
UPF, consumption mode	-1300	0	2600	0	Fig. 3
Non-UPF, generation mode	700	-1300	1300	2600	$\overset{\frown}{AB}$ of Fig. 4(a)

Fig. 12 shows the results in consumption mode and UPF control, and Fig. 13 shows the results in generation mode and non-UPF control.

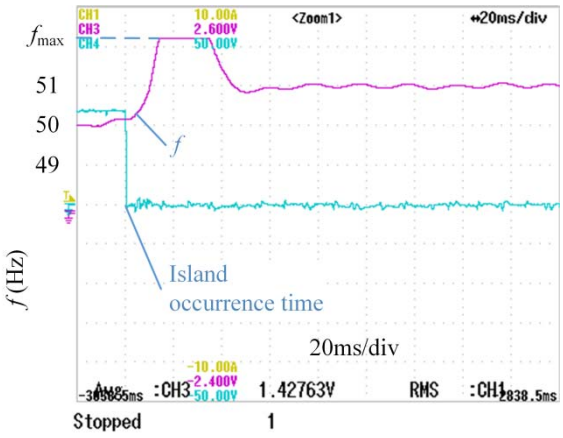

(a)

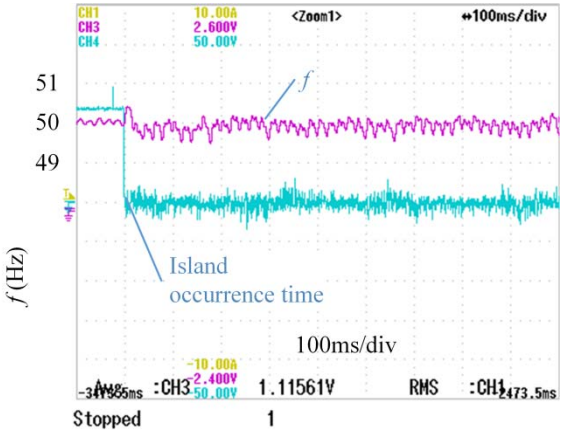

(b)

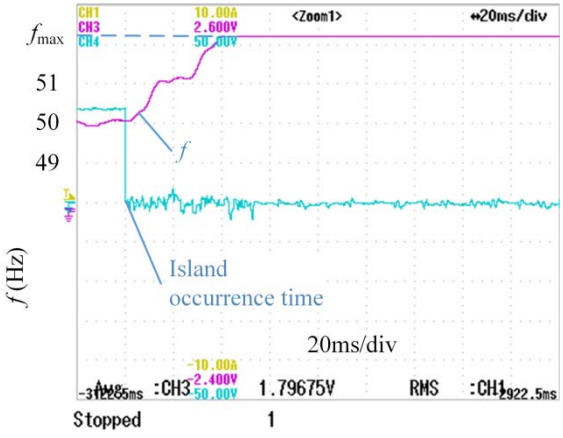

(c)

Fig. 12. Frequency waveforms in consumption mode and UPF control. (a) Improved method. (b) SFS with $d\theta_{con}/df > 0$. (c) SFS with $d\theta_{con}/df < 0$

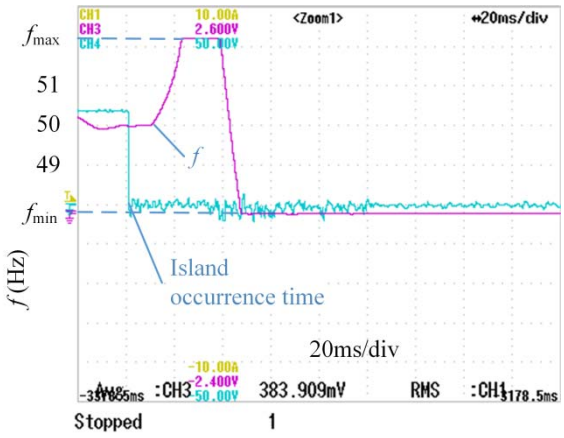

(a)

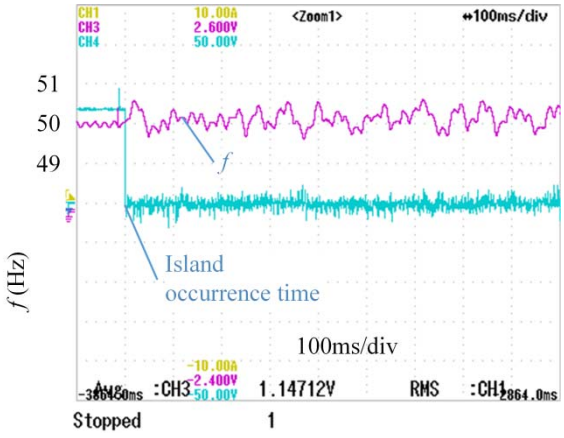

(b)

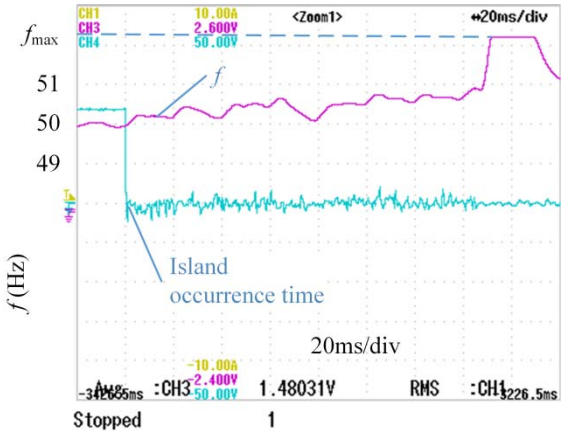

(c)

Fig. 13. Frequency waveforms in generation mode and non-UPF control. (a) Improved method. (b) SFS with $d\theta_{con}/df > 0$. (c) SFS with $d\theta_{con}/df < 0$

The frequency waveforms present obvious fluctuations in some figures, e.g. Fig. 13(b). However, the average is still within the normal range. To avoid misjudgment, generally there is a delay before the frequency fault is identified. In these experiments the fault will be identified when the frequency has been persistently out of the normal range for at least three grid periods (60 ms), so that the island will not be detected in such cases.

Accordingly, all the waveforms from the experiments are consistent with those from the simulations, which further strengthens the preceding conclusions.

VII. Conclusion

Through summarizing the conclusions in present literature, for frequency shift islanding detection methods a usable formula has been derived: the angle by which the total output current of the DR units leads the PCC voltage must be conducted to have the same shifting direction as the load admittance angle during the frequency variation. By introducing the formula into the classic frequency shift methods which is applied to the energy storage converter operating in multi-DR operations, it is found that the setting requirements of the angle by which the energy storage converter current leads the PCC voltage are inconsistent. As a result, the classic methods are applicable only in UPF control and have to distinguish between generation mode and consumption mode. For overcoming the shortcomings, an improved method applicable in every state has been proposed.

In generation mode, the operating characteristics of energy storage converters are similar to that of inverters. Therefore, the conclusions on frequency shift methods, which are based on energy storage converters in generation mode, are tenable for inverters as well. The modified schemes of the other frequency shift methods can be derived from the proposed usable formula if needed.

References

[1] X. Wang, W. Freitas, W. Xu, and V. Dinavahi, "Impact of DG Interface Controls on the Sandia Frequency Shift Antiislanding Method," *IEEE Trans. Energy Conversion*, vol. 22, no. 3, pp. 792-794, Sep. 2007.

[2] M. E. Ropp, M. Begovic, A. Rohatgi, G. A. Kern, R. H. Bonn, Sr., and S. Gonzalez, "Determining the Relative Effectiveness of Islanding Detection Methods Using Phase Criteria and Nondetection Zones," *IEEE Trans. Energy Conversion*, vol. 15, no. 3, pp. 290-296, Sep. 2000.

[3] A. Yafaoui, B. Wu, and S. Kouro, "Improved Active Frequency Drift Anti-islanding Detection Method for Grid Connected Photovoltaic Systems," *IEEE Trans. Power Electronics*, vol. 27, no. 5, pp. 2367-2375, May 2012.

[4] H. Vahedi, and M. Karrari, "Adaptive Fuzzy Sandia Frequency-Shift Method for Islanding Protection of Inverter-Based Distributed Generation," *IEEE Trans. Power Delivery*, vol. 28, no. 1, pp. 84-92, Jan. 2013.

[5] S. Akhlaghi, A. A. Ghadimi, and A. Akhlaghi, "A Novel Hybrid Islanding Detection Method combination of SMS and Q-f for Islanding Detection of Inverter- Based DG," in *Power and Energy Conference at Illinois*, Feb. 28-Mar. 1, 2014.

[6] G. Hung, C. Chang, and C. Chen, "Automatic Phase-Shift Method for Islanding Detection of Grid-Connected Photovoltaic Inverters," *IEEE Trans. Power Electronics*, vol. 18, no. 1, pp. 169-173, Mar. 2003.

[7] H. H. Zeineldin, "A Q–f Droop Curve for Facilitating Islanding Detection of Inverter-Based Distributed Generation," *IEEE Trans. Power Electronics*, vol. 24, no. 3, pp. 665-673, Mar. 2009.

[8] H. H. Zeineldin, E. F. El-Saadany, and M. M. A. Salama, "Islanding detection of inverter-based distributed generation," *IEE Proc.-Gener. Transm. Distrib.*, vol. 153, no. 6, pp. 644-652, Nov. 2006.

[9] S. Akhlaghi, A. Akhlaghi, and A. A. Ghadimi, "Performance analysis of the slip mode frequency shift islanding detection method under different inverter interface control strategy," in *Power and Energy Conference at Illinois (PECI), IEEE*, Illinois, USA, 19-20 Feb. 2016, pp. 1-7.

[10] S. Akhlaghi, H. Meshginkelk, A. Akhlaghi, and A. A. Ghadimi, "A novel hybrid islanding detection method for inverter based distributed generation based on frequency drift," *Australian Journal of Electrical & Electronics Engineering*, vol. 11, no. 2, pp. 161-174, 2014.

[11] H. H. Zeineldin, and J. L. Kirtley, "A Simple Technique for Islanding Detection With Negligible Nondetection Zone," *IEEE Trans. Power Delivery*, vol. 24, no. 2, pp. 779–786, Apr. 2009.

[12] Z. Ye, R. Walling, L. Garces, R. Zhou, L. Li, and T. Wang, "Study and Development of Anti-Islanding Control for Grid-Connected Inverters," General Electric Global Research Center, Niskayuna, New York, NREL/SR-560-36243, May 2004.

[13] Y. Jiao, Q. Song, and W. Liu, "Decoupled Instantaneous Current Control and Islanding Detection Strategy for a Single-Phase Photovoltaic Generation System," in *IECON 2010 - 36th Annual Conference on IEEE Industrial Electronics Society*, 7-10 Nov. 2010, pp. 210-3215.

[14] B. Kim, and S. Sul, "Comparison of Non-Detection Zone of Frequency Drift Anti-islanding with Closed-loop Power Controlled Distributed Generators," in *2015 IEEE 2nd International Future Energy Electronics Conference (IFEEC)*, Taipei, Taiwan, Nov. 2015, pp. 46-50.

[15] F. Lin, Y. Huang, K. Tan, J. Chiu, and Y. Chang, "Active islanding detection method using d-axis disturbance signal injection with intelligent control," *IET Gener. Transm. Distrib.*, vol. 7, no. 5, pp. 537-550, 2013.

[16] L. A. C. Lopes, and Y. Zhang, "Islanding Detection Assessment of Multi-Inverter Systems With Active Frequency Drifting Methods," *IEEE Trans. Power Delivery*, vol. 23, no. 1, pp. 480–486, Jan. 2008.

[17] M. A. Hosani, Z. Qu, and H. H. Zeineldin, "Scheduled Perturbation to Reduce Nondetection Zone for Low Gain Sandia Frequency Shift Method," *IEEE Trans. Smart Grid*, vol. 6, no. 6, pp. 3095-3103, Nov. 2015.

[18] H. H. Zeineldin, and S. Conti, "Sandia frequency shift parameter selection for multi-inverter systems to eliminate non-detection zone," *IET Renew. Power Gener.*, vol. 5, no. 2, pp. 175–183, 2011.

[19] X. Liu, P. Wang, and P. C. Loh, "A Hybrid AC/DC Microgrid and Its Coordination Control," *IEEE Trans. Smart Grid*, vol. 2, no. 2, pp. 278-286, Jun. 2011.

[20] D. Georgakis, S. Papathanassiou, N. Hatziargyriou, A. Engle, and C. Hardt, "Operation of a prototype Microgrid system based on micro-sources equipped with fast-acting power electronics interfaces," in *IEEE 35th Annual Power Electronics Specialists Conference*, Aachen, Germany, 2004, pp. 2521-2526.

[21] IEEE Standard Conformance Test Procedures for Equipment Interconnecting Distributed Resources with Electric Power Systems, IEEE Std 1547.1™-2005.

[22] M. J. E. Alam, K. M. Muttaqi, and D. Sutanto, "Mitigation of Rooftop Solar PV Impacts and Evening Peak Support by Managing Available Capacity of Distributed Energy Storage Systems," *IEEE Trans. Power Systems*, vol. 28, no. 4, pp. 3874-3884, Nov. 2013.

[23] M. B. Shadmand, R. S. Balog, and H. Abu-Rub, "Model Predictive Control of PV Sources in a Smart DC Distribution System: Maximum Power Point Tracking and Droop Control," *IEEE Trans. Energy Conversion*, vol. 29, no. 4, pp. 913-921, Dec. 2014.

[24] H. Sun, L. A. C. Lopes, and Z. Luo, "Analysis and Comparison of Islanding Detection Methods Using a New Load Parameter Space," in *The 3Mh Annual Conference of the IEEE Industrial Electronics Society*, Busan, Korea, 2004, pp. 1172-1177.

[25] H. H. Zeineldin, and S. Kennedy, "Sandia frequency-shift parameter selection to eliminate nondetection zones," *IEEE Trans. Power Delivery*, vol. 24, no. 1, pp. 486–487, Jan. 2009.

[26] M. E. Ropp, M. Begovic, and A. Rohatgi, "Prevention of Islanding in Grid-connected Photovoltaic Systems," *Progress in Photovoltaics*, vol. 7, pp. 39-59, 1999.

[27] F. Katiraei, and M. R. Iravani, "Power Management Strategies for a Microgrid With Multiple Distributed Generation Units," *IEEE Trans. Power Systems*, vol. 21, no. 4, pp. 1821-1831, Nov. 2006.

[28] Z. Zeng, H. Yang, and S. Tang, "Objective-Oriented Power Quality Compensation of Multifunctional Grid-Tied Inverters and Its Application in Microgrids," *IEEE Trans. Power Electronics*, vol. 30, no. 3, pp. 1255-1265, Mar. 2015.

[29] N. R. Tummuru, M. K. Mishra, and S. Srinivas, "Integration of PV/Battery Hybrid Energy Conversion System to the Grid with Power Quality Improvement Features," in *2013 IEEE International Conference on Industrial Technology*, 2013, pp. 1751-1756.

[30] A. Mohamed, V. Salehi, and O. Mohammed, "Reactive Power Compensation in Hybrid AC/DC Networks for Smart Grid Applications," in *The 3rd IEEE PES International Conference and Exhibition on Innovative Smart Grid Technologies*, Berlin, 2012, pp. 1-6.

[31] I. Wasiak, R. Pawelek, and R. Mienski, "Energy storage application in low-voltage microgrids for energy management and power quality improvement," *IET Gener. Transm. Distrib.*, vol. 8, no. 3, pp. 463–472, 2014.

[32] M. Falahi, S. Lotfifard, M. Ehsani, and K. Butler-Purry, "Dynamic Model Predictive-Based Energy Management of DG Integrated Distribution Systems," *IEEE Trans. Power Delivery*, vol. 28, no. 4, pp. 2217-2227, Oct. 2013.

[33] H. Vahedi, M. Karrari, and G. B. Gharehpetian, "Accurate SFS Parameter Design Criterion for Inverter-Based Distributed Generation," *IEEE Trans. Power Delivery*, vol. 31, no. 3, pp. 1050-1059, Jun. 2016.

[34] IEC standard frequencies, IEC 60196: 2009. [Online]. Available: https://webstore.iec.ch/publication/1017

Menghua Liu received a B.Eng degree in automatic control engineering from Wuhan University of Science and Technology, Wuhan, China, in 2005. He is currently pursuing a Ph.D. degree in electrical engineering at Tsinghua University, Beijing, China.

Before entering Tsinghua University he worked in a startup company focusing on new energy power generation, including wind turbine and photovoltaic power generation. His research interests include the control strategy of inverter/converter and fault detection techniques in distributed generation.

Wei Zhao received a Diploma degree in electrical engineering from Tsinghua University, Beijing, China, in 1982 and a Ph.D. degree from Moscow Power Engineering Institute Technical University, Moscow, Russia, in 1991.

He is currently a Professor with the Department of Electrical Engineering, Tsinghua University. His research interests include modern electromagnetic measurement and instrument techniques.

Songling Huang received a bachelor's degree in automatic control engineering from Southeast University, Nanjing, China, in 1991, and a Ph.D. degree in nuclear application technology from Tsinghua University, Beijing, China, in 2001.

He is currently a Professor with the Department of Electrical Engineering, Tsinghua University. His research interests include nondestructive evaluation and instrument techniques.

Qing Wang (SM'15) received a BEng in electronic instrument and measurement technique from Beihang University, Beijing, China, in 1995, an MSc in advanced manufacturing and materials from University of Hull, Hull, UK. in 1998, and a PhD in Manufacturing Management from De Montfort University, Leicester, U.K.in 2001.

She is currently an Associate Professor with the School of Engineering and Computing Sciences, Durham University, U.K. Her research interests include electronic instruments and measurement, computer simulation and advanced manufacturing technology.

Kunpeng Shi received a Master degree in electrical engineering from Northeast Dianli University, Jilin, China, in 2008. He is currently pursuing a Ph.D. degree in electrical engineering at Tsinghua University, Beijing, China.

He has been a senior engineer with the State Grid Jilinsheng electric power supply company. His research interests include new energy generation forecasting and optimal dispatching techniques.